ACS OMEGA

http://pubs.acs.org/journal/acsodf

Article

Coordination of Eu^{3+} Activators in ZnAlEu Layered Double Hydroxides Intercalated by Isophthalate and Nitrilotriacetate

Alysson F. Morais, Ivan G. N. Silva, Bonifácio C. Lima, Fernando A. Garcia, and Danilo Mustafa*

Cite This: *ACS Omega* 2020, 5, 23778−23785

Read Online

ACCESS | Metrics & More | Article Recommendations | Supporting Information

ABSTRACT: Luminescent layered double hydroxides (LDH) intercalated by isophthalate (ISO) and nitrilotriacetate (NTA) have been synthesized and characterized by powder X-ray diffraction (PXRD), extended X-ray absorption fine structure (EXAFS), elemental analysis (ICP-OES and CHN), and photoluminescence spectroscopy. While PXRD shows the successful formation of ZnAlEu LDHs, EXAFS reveals that the Eu activators are hosted in the hydroxide layers with an eightfold, oxygen-rich coordination, distinct from the sixfold coordination expected for the octahedral sites of metal cations in LDHs. This kind of coordination should locally distort the brucite-like layers. Additionally, the intercalation of ISO and NTA in the LDHs is shown to change the coordination environment around Eu compared to nitrate-intercalated ZnAlEu LDHs, which suggests that these anions directly interact with the Eu centers and/or strongly affect their coordination geometry. Finally, from the photoluminescence results, analyzed based on the Judd−Ofelt theory, it is determined that Eu is most likely in an environment with no inversion symmetry.

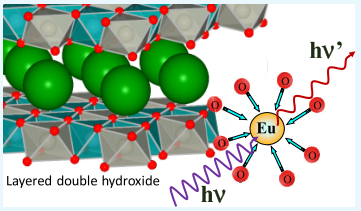

INTRODUCTION

Layered double hydroxides (LDH) are inorganic compounds with their structure based on the lamellar mineral brucite—$Mg(OH)_2$. Isomorphic substitution of divalent ions in the neutral brucite layer by tri- or tetravalent ions generates a positive layer charge that has to be compensated by adsorption of anions between the layers. This results in a general formula $[M_{1-x}^{II}M_{x}^{III}(OH)_2][A^{n-}]_{x/n}\cdot mH_2O$, such as in the natural mineral hydrotalcite, where part of the Mg^{II} is replaced by Al^{III}. LDH minerals exhibit a wide flexibility in composition and a score of polyvalent ions can be introduced into the layers.[1,2] The versatile composition of the LDH unlocks large application possibilities in diverse research fields, such as catalysis, electrolysis, drug delivery, and environmental sciences.[3−12]

Rare-earth (RE) elements are known for presenting unique luminescence properties attributed especially to their narrow emission lines and weak dependence of the emitted wavelengths to the host matrix. The explanation of these features resides in the shielding of the optically active partially filled 4f energy levels of the lanthanides provided by the completely filled external $5s^2$ and $5p^6$ subshells.[13−17] However, while the wavelength of the 4f−4f spectral lines of trivalent rare-earth (RE^{3+}) elements changes only a few nanometers when different matrices are compared, the relative intensity of their emission lines can be significantly modified by the crystal field, as described by the Judd−Ofelt theory.[18−27] According to this theory, the RE^{3+} 4f−4f transition probabilities are dependent on a set of three intensity parameters (Ω_2, Ω_4, and Ω_6), which depends on the odd components of the crystal-field potential. In general, Ω_2 is most affected by angular changes of the ligating atoms around the RE^{3+}, while Ω_4 and Ω_6 are more sensitive to radial changes and the polarizability of the groups coordinating to the RE^{3+}.[28] For Eu^{3+}, the Judd−Ofelt intensity parameters can be experimentally calculated from the integral intensity of the $(Eu^{3+})^5D_0 \rightarrow {}^7F_{1,2,4,6}$ 4f−4f electronic transitions.

The combination of RE^{3+} ions and layered double hydroxides is well reported in the literature and has been shown to produce interesting luminescent matrices. Other morphologies have also been obtained by the inclusion of RE^{3+} ions in the structure of LDHs, allegedly benefiting from the high coordination capacity of these elements to promote the selective alignment of the brucite-like layers over the surface of polymeric micelles.[1] Interlayer modifications in the LDHs have also been employed to tune and/or improve the luminescence properties of these materials. Examples are the intercalation of anionic photosensitizers to improve the overall luminescence of RE^{3+}-containing LDHs and the intercalation of luminescent complexes to create new luminescent phases. These approaches inspired the production of an enormous collection of RE^{3+}-based luminescent LDHs, including those intercalated by 4-biphenylacetate,[29] picolinate complexes,[30] β-diketonates,[31] trimesate,[2,31] and other carboxylates.[32]

Isophthalate is a benzenecarboxylate, a family of ligands known to be intramolecular energy donors for Eu^{3+}.[32,33]

Received: June 15, 2020
Accepted: August 25, 2020
Published: September 8, 2020

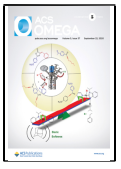

https://dx.doi.org/10.1021/acsomega.0c02848
ACS Omega 2020, 5, 23778−23785

Similarly, luminescence studies of Eu-nitrilotriacetate complexes (EuNTA) have shown that the triplet state of NTA (~29 000 cm^{-1}) can be used to populate the $^5D_0$ (~17 290 cm^{-1}) state of Eu^{3+}.[34] Then, intercalation of these two photosensitizers in Eu^{3+}-containing LDHs is expected to enhance the overall luminescence of these inorganic matrices. Additionally, nitrilotriacetic acid is a known chelating agent that, due to its wide use in detergents, fragrancies, plasters, polishes, and paints, is released to the environment. Hence, immobilization of nitrilotriacetate by its intercalation in LDHs is of interest for environmental remediation. Interestingly, nitrilotriacetate intercalated in LDHs can act as a solid-state chelating agent for metal ions in solution.[35,36] We also note that a MgAl LDH intercalated by nitrilotriacetate has been reported by Kaneyoshi et al.[37] and a ZnCr LDH hosting metal complexes of nitrilotriacetate in the interlayers has been reported by Gutmann et al.[35] Also, the long-lived triplet state of isophthalate anions intercalated in ZnAl LDHs has been recently shown to efficiently promote singlet oxygen generation under near-infrared absorption both in vitro and in vivo. Interestingly, the confined environment of ISO in the LDHs provides further stabilization for the triplet state of this photosensitizer.[38]

In this work, the synthesis and characterization of luminescent $Zn^{2+}/Al^{3+}/Eu^{3+}$ layered double hydroxides intercalated by isophthalate (ISO) and nitrilotriacetate (NTA) are described (see Figure 1). The coordination number of Eu^{3+} in

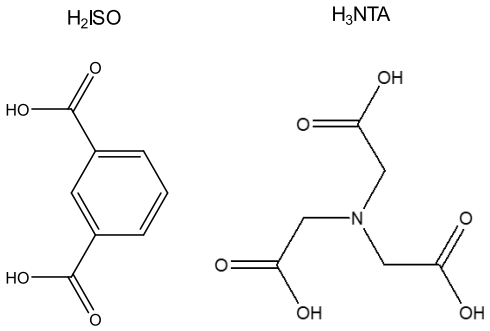

Figure 1. Acid forms of the ligands intercalated in the LDHs: benzene-1,3-dicarboxylic acid (H_2ISO, isophthalic acid), and nitrilotriacetic acid (H_3NTA).

the LDH matrices has been determined from Eu L^{III}-edge EXAFS measurements. The coordination changes occurring when the anionic species intercalated in the LDHs are replaced have been followed by the Judd–Ofelt intensity parameters obtained from the photoluminescence spectra. The intercalation of these carboxylates produces not only an increase in the noncentrosymmetric character of the Eu^{3+} site but also a modification in the polarizability of the electron cloud around this activator.

RESULTS AND DISCUSSION

Structural Properties. The powder X-ray diffraction (PXRD) patterns of LDH-ISO and LDH-NTA (Figure 2) confirm the formation of the LDH phase in both samples.[1,31,39] Their Bragg reflections can be indexed based on a three-layer hexagonal unit cell with rhombohedral centering. In the lower angle region, $2\theta < 25°$, the (00l) Bragg peaks of each pattern arise from the reflections coming from the basal planes passing through the metal sites in the hydroxide layers. Especially, the

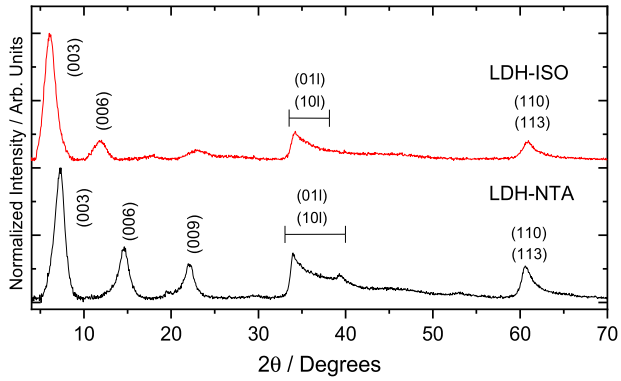

Figure 2. PXRD patterns of the samples LDH-ISO and LDH-NTA indexed based on a three-layer hexagonal unit cell.

$d_{(003)}$ planar distance corresponds to the basal spacing of each clay structure, comprising the interlayer spacing and the thickness of the hydroxide layer.

The summary of the main features derived from the PXRD analysis is presented in Table 1. The intercalation of ISO and NTA expands the interlayer gallery of these clays compared to nitrate-intercalated materials, which makes the basal reflections of LDH-ISO and LDH-NTA to appear shifted to lower angles. The interlayer distance in LDH-ISO is larger than that of LDH-NTA. Estimating the thickness of the hydroxide layer as 4.8 Å, the interlayer spacing of the clay structures is calculated to be 9.8 and 7.2 Å for LDH-ISO and LDH-NTA, respectively. For LDH-ISO, these values are consistent with a bridging orientation for the interlayer anion, where each terminal COO^- interacts with a different hydroxide layer. For LDH-NTA, both the parallel and the bridging orientations are possible by considering the size of nitrilotriacetate.

For both LDH-ISO and LDH-NTA, the first basal reflection is more intense than the second ($I(003) > I(006)$), which suggests that Eu^{3+} is not immobilized as a metal complex in the interlayers. In general, inversion of this feature is observed when heavy metal cations are present in the interlayer medium, located near to the midpoint of the interlayer gallery.[40] This feature has been attributed to an increase in the electron density at the midpoint of the c axis, which constructively contributes to the (006) reflection, but destructively contributes to $I(003)$.

In the angular region from 2θ = 30 to 40°, a broad and asymmetric peak formed by an envelope of (01l) and (10l) reflections is observed in the PXRD patterns of LDH-ISO and LDH-NTA. The appearance of this asymmetric feature has been described elsewhere to be indicative of local distortions within the brucite-like layers.[41] A last diffraction feature is observed at $2\theta \sim 60.9°$ for both samples, corresponding to the superposition of the (110) and (113) Bragg reflections, which, for layered structures with large basal spacing, appear superposed. Since the $d_{(110)}$ planar distance is related to the average metal-to-metal distance within the hydroxide layers—"$a_{MM} = 2d_{(110)}$"—a_{MM} is estimated to be 3.06 Å. This value matches the Zn–Al distance in ZnAl LDHs with metal fraction Zn/Al = 2. Since it is known from the LDH literature that a_{MM} strongly correlates with the M^{II}/M^{III} metal fraction in the layered phase, with a_{MM} increasing with a decrease in the Al content, a M^{II}/M^{III} ratio close to 2 is expected in the layered phase of the samples LDH-ISO and LDH-NTA.[41]

https://dx.doi.org/10.1021/acsomega.0c02848
ACS Omega 2020, 5, 23778–23785

Table 1. Crystallographic Properties of LDH-ISO and LDH-NTA and Estimate for the Dimensions of the Intercalated Anions

sample	$2\theta_{003}$ (deg)[a]	$\delta(2\theta_{003})$ (deg)[b]	$d_{(003)}$ (Å)[c]	$L_{(003)}$ (Å)[d]	interlayer distance (Å)[e]	anion dimensions (Å)[f]
LDH-ISO	6.06	1.54	14.6	54.0	9.8	6.9 × 4.9 × 2.2
LDH-NTA	7.26	1.37	12.0	60.7	7.2	5.1 × 5.7 × 4.2

[a]Peak position. [b]Full width at half-maximum. [c]Basal spacing. [d]Scherrer crystallite size in the (003) direction for a Gaussian peak; instrumental width: 0.14° 2θ. [e]Basal spacing minus the thickness of the hydroxide layer estimated as 4.8 Å. [f]An estimate for the height × width × thickness of ISO and NTA in the geometry shown in Figure 1.

Chemical Composition. Bulk analysis of the elemental composition of LDH-ISO and LDH-NTA has been investigated by ICP-OES and CHN. The empirical formula of the precipitates has been written assuming that (1) carboxylates are the only source of carbon; (2) for LDH-ISO, nitrogen originated from nitrate ions in the samples; and (3) the excess of nitrogen in LDH-NTA originated from nitrate anions.

LDH-ISO. Anal. Calcd. for $[Zn_2Al_{1.14}Eu_{0.050}(OH)_{6.38}]$-$[(NO_3^-)_{0.010}(ISO^{2-})_{0.45}(Na^+)_{0.10}]$ – wt % Calc.: Zn, 36.34; Al, 8.55; Eu, 2.11; Na, 0.64; C, 12.00; H, 2.27; N, 0.39. Found: Zn, 36.49; Al, 8.61; Eu, 2.10; Na, 0.75; C, 11.95; H, 3.31; N, 0.38.

LDH-NTA. Anal. Calcd. for $[Zn_2Al_{1.08}Eu_{0.045}(OH)_{6.25}]$-$[(NO_3^-)_{0.24}(NTA^{2-})_{0.41}(Na^+)_{0.07}]\cdot 0.88H_2O$ – wt % Calc.: Zn, 34.10; Al, 7.60; Eu, 1.78; Na, 0.42; C, 7.70; H, 2.84; N, 2.41. Found: Zn, 34.00; Al, 7.61; Eu, 1.77; Na, 0.59; C, 7.69; H, 3.12; N, 2.35.

The M^{II}/M^{III} metal fractions for LDH-ISO (1.75) and LDH-NTA (1.85) are lower than the minimum theoretical fraction of 2 allowed by the Pauli principle, the so-called cation avoidance rule. This suggests the precipitation of Al impurities in the samples.[42] The same conclusion arises from the charge unbalance resulting from the empirical formulas if one considers all Al to be hosted in the hydroxide layers of the LDH phases. Assuming that the true Al content in the LDHs is defined by the charge balance in the materials, we expect that 0.24 and 0.09 moles of Al per unit formula precipitate as impurity phases in LDH-ISO and LDH-NTA, respectively. We note that the formation of gibbsite, boehmite, and amorphous Al hydroxide or oxohydroxide phases is not uncommon in the synthesis of LDHs.[42] For instance, other studies on NTA-intercalated LDHs also reported bulk M^{II}/M^{III} fractions lower than 2, which was associated with the formation of boehmite, as observed by powder X-ray diffraction.[37] In the case of LDH-ISO and LDH-NTA, no additional phase could be detected in their PXRD patterns, showing that the excess Al is precipitated in an amorphous phase. The amounts of ISO and NTA found in the samples indicate that these anions are intercalated in the LDHs as ISO^{2-} and NTA^{2-}, which is understood given that the synthesis pH is around pH 8, and $pK_{a1,2}$(ISO) = 3.30, 4.38 and $pK_{a1,2,3}$(NTA) = 1.89, 2.49, and 9.37.[37,43−45]

While isophthalate has shown a strong preference to be intercalated in the LDHs in the expense of nitrate, which is also present during the synthesis, nitrilotriacetate is intercalated together with a considerable amount of this monovalent anion. The Eu/(Al + Eu) fraction in the samples is slightly lower than the nominal fraction of 5% added for the synthetic procedure.

X-ray Absorption Spectroscopy (XAS). To characterize the coordination environment around the Eu^{3+} activators in LDH-ISO and LDH-NTA, Eu L^{III}-edge XAS data were collected and analyzed. In the XANES part of the spectrum (Figure 3), the most intense absorption feature is centered at 6983.1 eV, corresponding to the Eu(III) oxidation state. No

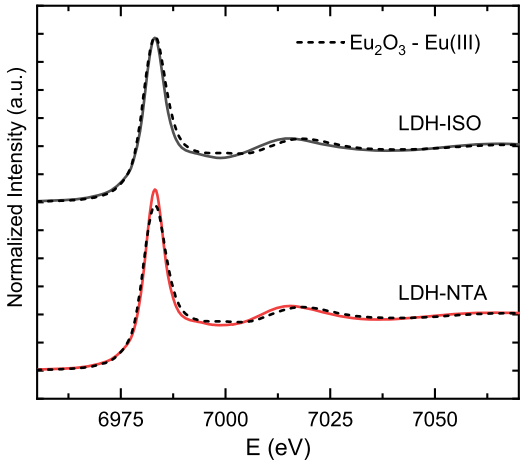

Figure 3. Normalized Eu L^{III}-edge near-edge spectra (XANES) for LDH-ISO and LDH-NTA. The spectrum of Eu_2O_3, a reference compound featuring only Eu(III), has been measured for comparison.

absorption feature corresponding to Eu(II), expected at around 6975 eV,[46] has been found.

Figure 4 displays the EXAFS part of the XAS spectra along with the Fourier transformed data. The similarity between the data for LDH-ISO and LDH-NTA suggests that Eu is in a similar environment in both samples. A single-shell fit to the k^3-weighted EXAFS data for LDH-ISO and LDH-NTA reveals, respectively, an average number of 7.7 and 7.8 oxygen atoms at around 2.429 and 2.431 Å (Table 2), which are likely to be ascribed to water and/or hydroxyl groups bonded to Eu and possibly to oxygen from the COO^- groups that may directly bind to the metal centers in the LDHs. The second and third coordination shells observed on the Fourier transformed data could be well described by oxygen and zinc scatterers at around 3.6 and 4.0 Å, respectively. With this Eu−Zn distance and considering the thickness of a hydroxide layer to be around 4.8 Å, the accommodation of eightfold-coordinated europium surrounded to oxygen atoms at a distance of 2.4 Å can only happen if Eu is hosted within the brucite-like layers. In this case, a Eu−Zn distance longer than that expected for the metal sites in ZnAl LDHs (~3.06 Å) shows that the inclusion of Eu distorts the hydroxide layers. No signal from Eu backscatters has been found in the EXAFS data, thus ruling out the segregation of this cation in Eu-rich phases such as $Eu(OH)_3$ and EuO(OH).

Infrared and Photoluminescence Spectroscopy. To characterize the functional groups present in the samples, the infrared transmittance spectra of LDH-ISO and LDH-NTA were measured (see Figure 5). In the high-wavenumber region, the broad bands comprising the absorption maxima at approximately 3400 cm^{-1} are due to the O−H stretching vibrations of the interlayer and surface water and structural hydroxides. High intensity and large width of this band are expected due to the high degree of hydration and the presence

https://dx.doi.org/10.1021/acsomega.0c02848
ACS Omega 2020, 5, 23778−23785

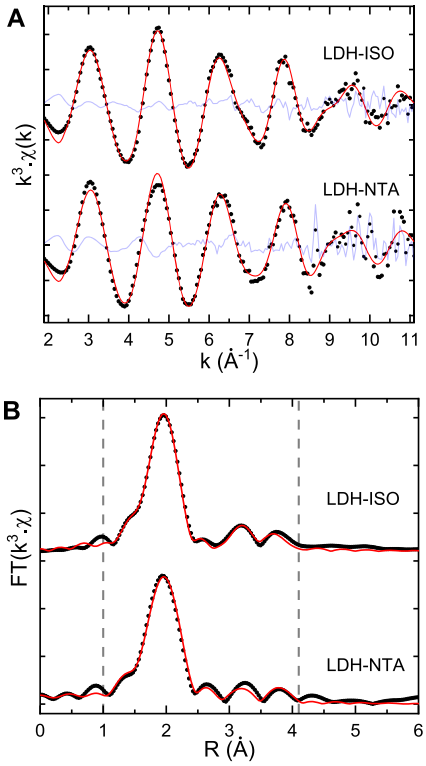

Figure 4. (A) Eu L^{III}-edge EXAFS spectra and (B) Fourier transformed data for LDH-ISO and LDH-NTA. The black circles, the red, and the faint blue lines represent the data, the fit, and the residuals, respectively.

Table 2. Structural Parameters Refined from EXAFS[a]

sample	shell	CN[b]	R (Å)[c]	σ^2 (Å²)[d]
LDH-ISO	Eu−O	7.7(4)	2.429(4)	0.0095(7)
	Eu−O	3.3(9)	3.65(1)	0.0048(29)[f]
	Eu−Zn	6[e]	4.03(2)	0.024(3)[f]
LDH-NTA	Eu−O	7.8(7)	2.431(5)	0.0099(11)
	Eu−O	2.4(9)	3.62(3)	0.0048(29)[f]
	Eu−Zn	6[e]	3.99(3)	0.024(3)[f]

[a]Amplitude reduction factor: S_0^2 = 0.95 (see the Experimental Section). Energy shift: ΔE = (3.4 ± 0.4) eV. R-factor = 0.67%. Fitting range: 2.0 < k < 10.5 Å^{-1}, 1.0 < R < 4.1 Å. [b]Coordination number. [c]Bond distance. [d]Debye−Waller factor. [e]Not floated. [f]Variables constrained during the fit.

of slightly different biding energies in the O−H oscillators in the systems.

The bands appearing in the range of 1350−1650 cm^{-1} are attributed to the interlayer carboxylate groups. The exact wavelength determination for the symmetrical vibrations of these O═C═O groups is complicated by the presence, in the same region, of the N−O vibration corresponding to the very sharp feature at 1384 cm^{-1}. The presence of this absorbing mode for all samples confirms the elemental analyses data, indicating that the carboxylates do not completely replace the nitrate anions in the interlayers of the investigated materials.

To tentatively infer the coordination modes of the interlayer carboxylates, the IR spectra of LDH-ISO and LDH-NTA have been compared to those of the sodic salts Na_2ISO and Na_3NTA (faint lines in Figure 5), which were prepared by neutralization of the acid ligands with sodium hydroxide. A comparison of the wavelength difference $\Delta = \nu_{as} - \nu_s$ between

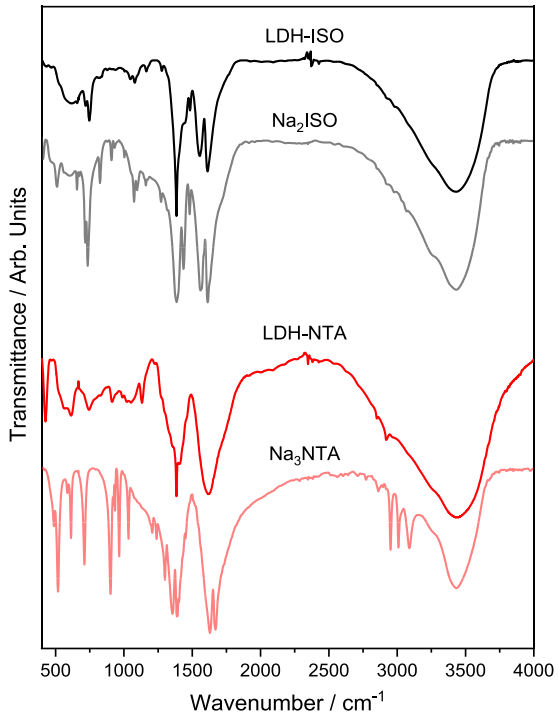

Figure 5. Infrared transmittance spectra of LDH-ISO and LDH-NTA dispersed in KBr pellets.

the asymmetric and symmetric vibrational modes of the carboxylate groups in the LDH precipitates and in the sodic salts (Δ_{Ionic}) was employed. For $\Delta > \Delta_{Ionic}$, $\Delta \ll \Delta_{Ionic}$, and $\Delta \lesssim \Delta_{Ionic}$, monodentate, chelating, and bridging bidentate coordination are assigned, respectively.[47,48]

In the spectral region from 1350 to 1600 cm^{-1}, very similar profiles are observed for LDH-ISO and Na_2ISO, except for the presence of the very sharp absorption of nitrate. The symmetric and asymmetric vibrational modes of the carboxylate groups are observed at 1385 and 1630 cm^{-1}, respectively.[49] The large difference Δ = 245 cm^{-1}, similar to that of the sodic salt, combined with the splitting in the ν_s band, suggests a mixed bridging bidentate and chelate coordination for the isophthalate interlayer anion. For the carboxylate groups of NTA, the narrow absorption peaks observed in Na_3NTA appear broaden in the spectra of LDH-NTA, which could suggest the existence of more than one coordination mode for these anions. This explanation is further supported by the partial deprotonation expected for NTA in the pH of synthesis (pH 8), which then provides at least two coordination environments. Also, we note that all of the metal cations in the samples (Zn, Al, and Eu) may function as binding centers for the interlayer anions, which is likely to further contribute to line broadening. The asymmetric vibrational mode of the carboxylate groups of LDH-NTA (1620 cm^{-1}) appears shifted to lower wavenumbers compared to Na_3NTA (1673 cm^{-1}) and produces $\Delta \ll \Delta_{Ionic}$, suggesting the existence of a chelate binding mode for this anion. We note that both chelate and monodentate coordination and even no coordination to the metallic centers in layered hydroxides have already been observed for carboxylates intercalated in layered phases. Interestingly, Shao et al.[50] have shown that the Eu^{3+}−COO^- binding in layered rare-earth hydroxides intercalated with (hetero)aromatic carboxylates enhances the photoluminescence (PL) properties of Eu^{3+}, while no effect on PL

https://dx.doi.org/10.1021/acsomega.0c02848
ACS Omega 2020, 5, 23778−23785

is observed when these carboxylates are not coordinated to the metallic center.

The photoluminescence spectra of LDH-ISO and LDH-NTA are shown in Figure 6. The excitation spectra (Figure 6A) were obtained by monitoring the $(Eu^{3+})^5D_0 \rightarrow {}^7F_2$ emission at 614 nm. A broad band from 240 to 350 nm is observed in the excitation spectra, corresponding to singlet−singlet transitions ($S_0 \rightarrow S_n$) of each carboxylate with subsequent energy transfer to the $(Eu^{3+})^5D_0$ state.[33,34] Also visible are the sharp excitation bands corresponding to 4f−4f intraconfigurational transitions of Eu^{3+}. For LDH-ISO, the high-intensity ligand-to-metal excitation band shows that the activator is more efficiently sensitized by indirect excitation, with isophthalate as an antenna. On the other hand, for LDH-NTA, direct excitation of Eu^{3+} is observed to be the most efficient.

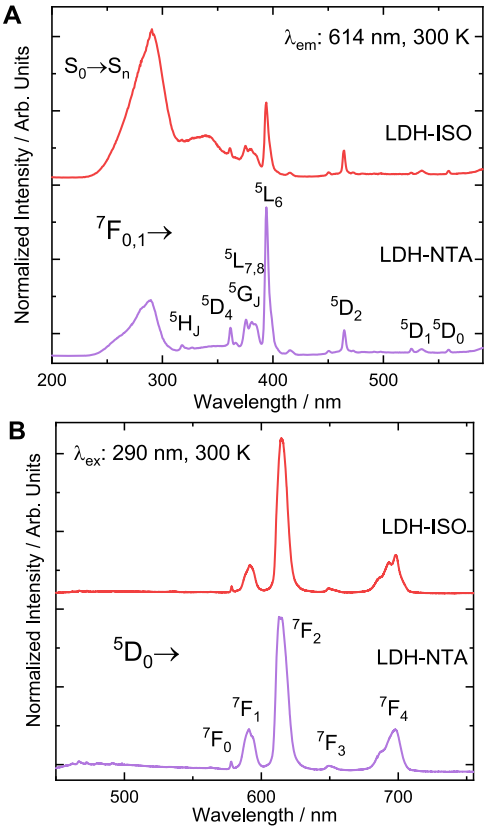

Figure 6. Excitation spectra monitored at 614 nm (A) and emission spectra (B) with excitation at the peak intensity of the $S_0 \rightarrow S_n$ band (290 nm). The 4f−4f transitions in Eu^{3+} are indicated by the term symbols of the 4f electronic states.

The emission spectra (Figure 6B) of LDH-ISO and LDH-NTA show the sharp emission bands characteristic of the 4f−4f transitions in Eu^{3+}. In the range 450−550 nm, the absent or low-intensity emission of ISO and NTA shows the excellent ligand → Eu^{3+} nonradiative energy transfer in the samples and reveals the proximity between Eu and the carboxylates in the system.[51,52] The relative intensity of the observed emissions shows information about the coordination symmetry around the Eu centers. In fact, since the $(Eu^{3+})^5D_0 \rightarrow {}^7F_2$ emission is the most intense for both samples, it is most likely that Eu^{3+} is in a site with no inversion symmetry. In noncentrosymmetric ligand fields, Laporte's rule for the 4f−4f transitions is partially relaxed by the mixing of electronic configurations with an opposite parity caused by the existence of odd components in the crystal field. This mechanism makes the $(Eu^{3+})^5D_0 \rightarrow {}^7F_{2,4}$ transitions appear enhanced, more intense than the magnetic dipole transition $(Eu^{3+})^5D_0 \rightarrow {}^7F_1$.[53,54]

More information on the local symmetry around the Eu^{3+} activators in LDH-ISO and LDH-NTA can be obtained by analyzing the experimental Judd−Ofelt intensity parameters ($\Omega_{2,4}$) for these samples. Ω_2 and Ω_4 are calculated from the emission intensity ($S_{1,2,4}$) and the barycenter ($\lambda_{1,2,4}$) of the $(Eu^{3+})^5D_0 \rightarrow {}^7F_{1,2,4}$ transitions in the emission spectra as

$$\Omega_{2,4} = \frac{D_{MD}\,\lambda_{2,4}^4}{e^2\,\lambda_{MD}^4\,U_{2,4}}\,\frac{9\,n^3}{n(n^2+2)^2}\,\frac{S_{2,4}}{S_1} \quad (1)$$

where the reduced dipole matrices $U_{2,4}$ and the dipole strength of the magnetic dipole transition $(Eu^{3+})^5D_0 \rightarrow {}^7F_1$, $D_{MD} = 9.6 \times 10^{-6}$ debye^2, are tabulated quantities[14,55] and e is the elementary electric charge. The refractive index of the matrix, n, has been assumed to be 1.5 in accordance with other investigations.[40,56] While Ω_2 is more sensitive to angular changes in the first coordination shell around Eu^{3+}, Ω_4 is more influenced by radial movements and the polarizability of the ions in the neighborhood of this activator.[13,57] In addition, the total radiative transition rate of the $Eu^{3+}(^5D_0)$ electronic state, A_{rad}, is determined as

$$A_{rad} = A_1 + \sum_{J=2,4} \frac{64\,e^2\,\pi^4}{3h\,(2J+1)\lambda_J^3}\,\frac{n(n^2+2)^2}{9}\,\Omega_J\,U_J \quad (2)$$

where the radiative transition rate of the magnetic dipole transition $(Eu^{3+})^5D_0 \rightarrow {}^7F_1$ is $A_1 = 50\ s^{-1}$.[14,14]

The experimental Judd−Ofelt parameters, $\Omega_{2,4}$, along with the radiative decay rates, A_{rad}, for the $^5D_0$ emitting level of the Eu activators in LDH-ISO and LDH-NTA are shown in Table 3. Data from LDHs intercalated by other ligands and published elsewhere are shown for comparison. We note that the photoluminescence properties of the LDHs are modified when the anions intercalated in these materials are changed, which indicates that the coordination symmetry around Eu is dependent on the intercalated anion. Among the ZnAlEu LDHs described in the literature, the nitrate-intercalated material is found to show the lowest value for both Ω_2 and Ω_4, thus suggesting that the intercalation of ISO and NTA creates a less centrosymmetric chemical environment for Eu. Similar conclusions have been drawn for the intercalation of other carboxylates and also for β-diketones.[31]

Table 3. Experimental Intensity Parameters ($\Omega_{2,4}$) and Radiative Transition Rate (A_{rad})

sample	Ω_2 (10^{-20} cm^2)	Ω_4 (10^{-20} cm^2)	A_{rad} (s^{-1})
LDH-ISO	11.6 ± 0.9	10 ± 1	546
LDH-NTA	8.1 ± 0.7	7.1 ± 0.8	399
LDH-ACAC[a]	14.4 ± 0.4	8.1 ± 0.2	608
LDH-TTA[a]	14.0 ± 0.3	7.8 ± 0.2	591
LDH-BTC[a]	10.3 ± 0.2	10.0 ± 0.2	504
LDH-NO_3^-[a]	3.9 ± 0.1	1.8 ± 0.1	192

[a]Reference 31. ACAC = acetylacetonate. TTA = thenoyltrifluoroacetonate. BTC = 1,3,5-benzenetricarboxylate.

As shown in Table 3, Ω_2 increases in the order LDH-NO_3^- < LDH-NTA < LDH-BTC ≲ LDH-ISO < LDH-TTA = LDH-

https://dx.doi.org/10.1021/acsomega.0c02848
ACS Omega 2020, 5, 23778−23785

ACAC, suggesting that a less centrosymmetric environment is created around Eu by the intercalation of the organic anions. Considering the error bars, similar values are obtained for both Ω_2 and Ω_4 in the LDHs intercalated by the carboxylates ISO and BTC, thus suggesting that the symmetry around the activator is essentially influenced by the radicals directly interacting with hydroxide layers, regardless of other details of the anions. The same feature is observed for the LDHs intercalated by the β-diketones ACAC and TTA. For LDH-NTA, we note that large amounts of nitrate have been found to co-intercalate in the LDHs together with NTA. This creates a mixture of more than one environment for the Eu centers in this material, which presents an intermediate value for the Judd−Ofelt parameters: LDH-NO_3^- < LDH-NTA < LDH-ISO.

CONCLUSIONS

In summary, isophthalate (ISO) and nitrilotriacetate (NTA) have been shown to successfully intercalate in ZnAlEu layered double hydroxides. In the case of LDH-NTA, the interlayer gallery is occupied by both NTA and nitrate, the second being originated from the metal precursor salts. This co-intercalation is less pronounced in LDH-ISO.

The coordination of the Eu centers in the LDHs has been shown to be constituted by eight oxygen atoms at around 2.43 Å. EXAFS analysis is supportive of the presence of Eu^{3+} in the hydroxide layers. Although it is hard to determine the exact geometry of the Eu site, it is known from the photoluminescence studies that Eu is most likely in an environment with no inversion symmetry. This feature clearly distinguishes the Eu site against the sixfold octahedral coordination found for Zn, Al, and most of the metals hosted in LDHs. A direct consequence of this distinct coordination is that the inclusion of Eu in the LDHs should locally distort the hydroxide layers of these materials.

The intercalation of ISO and NTA in the LDHs is shown to have an important impact on the coordination of Eu, which affects the Judd−Ofelt parameters. A comparison between Ω_2 and Ω_4 for LDH-ISO and LDH-NTA and the values presented in the literature for nitrate-intercalated ZnAlEu LDHs shows that intercalation of ISO and NTA sets up a less centrosymmetric chemical environment for Eu. A similar effect has been found for the intercalation of other carboxylates and also for β-diketones, suggesting that these anions directly interact with the Eu centers hosted in the LDHs and/or strongly affect the coordination geometry around Eu.

EXPERIMENTAL SECTION

The metal precursors used were $Zn(NO_3)_2{\cdot}6H_2O$ (98 mol %, Vetec), $Al(NO_3)_3{\cdot}9H_2O$ (98 mol %, LabSynth), and $Eu(NO_3)_3{\cdot}6H_2O$ (prepared from Eu_2O_3 − CSTARM, 99,99 mol %—by addition of concentrated nitric acid). NaOH (97 mol %, Vetec), H_3NTA (99 mol %, Sigma-Aldrich), and H_2ISO (99 mol %, Sigma-Aldrich) were purchased and used without further purification (see Figure 1).

Synthetic Procedure. ISO- and NTA-intercalated Eu^{3+}-doped Zn^{2+}/Al^{3+} layered double hydroxides (LDH-ISO and LDH-NTA) were prepared by coprecipitation of the metal cations at constant pH. To prepare the LDHs, a 10 mL aqueous solution containing the metal salts $Zn(NO_3)_2$, $Al(NO_3)_3$, and $Eu(NO_3)_3$ at concentrations of 0.667, 0.317, and 0.0167 mol·L^{-1}, respectively, was added dropwise (~10 mL·h^{-1}) to a 200 mL solution containing dissolved anions in excess to neutralize the positive charge of the hydroxide layers. The pH was permanently kept between pH 7.8 and pH 8.2 by dosing a 1 mol·L^{-1} NaOH solution with the automatic titrator Metrohm 785 DMP. At this pH, both ISO and NTA are doubly charged: $pK_{a1,2}$(ISO) = 3.30 and 4.38; $pK_{a1,2,3}$(NTA) = 1.89, 2.49, and 9.37.[37,43−45] ISO and NTA concentrations used were 16.6 and 11.1 mmol·L^{-1}, respectively. In the final mother liquid, these concentrations produce the following molar fractions: Zn/(Al + Eu) = 2, Eu/(Al + Eu) = 0.05, NTA/(Al + Eu) = 2/3, and ISO/(Al + Eu) = 1. After the dosing of the metal solution was finished, the resulting mixture was aged statically at 60 °C for 2 days to optimize crystallization. At the end, the final slurry was submitted to a washing procedure following centrifugation, rinsing with distilled water, and drying in an oven at 60 °C for 3 days. A fine powder was obtained by grinding the solid with a mortar and pestle.

Characterization. The samples were submitted to elemental analysis to determine the aluminum, zinc, europium, sodium, carbon, hydrogen, and nitrogen contents. For CHN analysis, a PerkinElmer (Massachusetts, EUA) 2400 Series II elemental analyzer was used. For the metal content, inductively coupled plasma optical emission spectrometry (ICP-OES) was performed in a Spectro Arcos analyzer (SPEXTRO Analytical Instruments GmbH, Germany). Powder X-ray diffraction (PXRD) patterns were acquired using a Cu Kα, 1.5418 Å Bruker D8 (Massachusetts, EUA) diffractometer. Infrared absorption spectroscopy was performed using the KBr pellets technique in an ABB Bomem (Zurich, Switzerland) MB100 FTIR spectrometer. Scanning electron microscopy (SEM) images were obtained using a field emission JEOL (Tokyo, Japan) JSM 7401F. Photoluminescence studies of the samples were carried out using a 450 W xenon lamp and two 0.22 m double-grating SPEX 1680 monochromators SPEX FL212 Fluorolog-3 (Horiba, Kyoto, Japan) spectrofluorometer. All spectra were corrected for the intensity profile of the xenon lamp and detection response. Eu L^{III}-dge X-ray absorption near-edge structure (XANES) and extended X-ray absorption fine structure (EXAFS) data were collected at the XAFS2[58] beamline of the Brazilian Synchrotron Light Laboratory (LNLS, Campinas, Brazil). For the analysis of the Eu L^{III}-edge EXAFS data for the LDHs, layered rare-earth hydroxides[59] (LREH) have been used as crystal analogues for the calculations implemented in the Demeter platform.[60] An amplitude reduction factor S_0^2 = 0.95 ± 0.11 has been obtained from the fitting of the Eu L^{III}-edge EXAFS data for the model compound Eu_2O_3 (cubic phase,[61] coordination number = 6; see Figure S1). Chemical transferability was assumed, and this amplitude factor has been used in the analysis of the LDH samples.

ASSOCIATED CONTENT

Supporting Information

The Supporting Information is available free of charge at https://pubs.acs.org/doi/10.1021/acsomega.0c02848.

EXAFS data and fit for the reference material Eu_2O_3 (Figure S1) (PDF)

AUTHOR INFORMATION

Corresponding Author

Danilo Mustafa − *Departamento de Física dos Materiais e Mecânica, Instituto de Física da Universidade de São Paulo, São*

https://dx.doi.org/10.1021/acsomega.0c02848
ACS Omega 2020, 5, 23778−23785

Paulo, SP 05508-090, Brazil; orcid.org/0000-0001-5453-1737; Email: dmustafa@if.usp.br

Authors

Alysson F. Morais − *Departamento de Física dos Materiais e Mecânica, Instituto de Física da Universidade de São Paulo, São Paulo, SP 05508-090, Brazil;* orcid.org/0000-0001-7463-7432

Ivan G. N. Silva − *Departamento de Física dos Materiais e Mecânica, Instituto de Física da Universidade de São Paulo, São Paulo, SP 05508-090, Brazil;* orcid.org/0000-0002-9382-1080

Bonifácio C. Lima − *Departamento de Física dos Materiais e Mecânica, Instituto de Física da Universidade de São Paulo, São Paulo, SP 05508-090, Brazil*

Fernando A. Garcia − *Departamento de Física Aplicada, Instituto de Física da Universidade de São Paulo, São Paulo, SP 05508-090, Brazil;* orcid.org/0000-0001-5694-640X

Complete contact information is available at: https://pubs.acs.org/10.1021/acsomega.0c02848

Notes

The authors declare no competing financial interest.

■ ACKNOWLEDGMENTS

The authors acknowledge the Laboratory of Crystallography (IFUSP, São Paulo) for assistance with the PXRD measurements and CNPEM-LNLS for the concession of beamtime (proposal nos. 20190148 and 20180133). The CNPEM-LNLS staff are acknowledged for technical assistance during experiments. Victoria Valentim Freire and Dimy Nanclares are acknowledged for assistance during the experiments at the XAFS2 beamline. This research was funded by Fundação de Amparo à Pesquisa do Estado de São Paulo (FAPESP, 2015/19210-0 and 2018/13837-0), Coordenação de Aperfeiçoamento de Pessoal de Nível Superior (CAPES, 1723707, Finance Code 001), and Conselho Nacional de Desenvolvimento Científico e Tecnológico (CNPq, 142127/2014-0 and 403055/2016-4).

■ REFERENCES

(1) Morais, A. F.; Silva, I. G. N. N.; Sree, S. P.; de Melo, F. M.; Brabants, G.; Brito, H. F.; Martens, J. A.; Toma, H. E.; Kirschhock, C. E. A. A.; Breynaert, E.; Mustafa, D. Hierarchical Self-Supported ZnAlEu LDH Nanotubes Hosting Luminescent CdTe Quantum Dots. *Chem. Commun.* **2017**, *53*, 7341−7344.

(2) Teixeira, A.; Morais, A.; Silva, I.; Breynaert, E.; Mustafa, D. Luminescent Layered Double Hydroxides Intercalated with an Anionic Photosensitizer via the Memory Effect. *Crystals* **2019**, *9*, 153.

(3) Khan, A. I.; O'Hare, D. Intercalation Chemistry of Layered Double Hydroxides: Recent Developments and Applications. *J. Mater. Chem.* **2002**, *12*, 3191−3198.

(4) Fan, G.; Li, F.; Evans, D. G.; Duan, X. Catalytic Applications of Layered Double Hydroxides: Recent Advances and Perspectives. *Chem. Soc. Rev.* **2014**, *43*, 7040−7066.

(5) Santos, R. M. M.; Tronto, J.; Briois, V.; Santilli, C. V. Thermal Decomposition and Recovery Properties of ZnAl−CO_3 Layered Double Hydroxide for Anionic Dye Adsorption: Insight into the Aggregative Nucleation and Growth Mechanism of the LDH Memory Effect. *J. Mater. Chem. A* **2017**, *5*, 9998−10009.

(6) Zhang, S.; Yao, F.; Yang, L.; Zhang, F.; Xu, S. Sulfur-Doped Mesoporous Carbon from Surfactant-Intercalated Layered Double Hydroxide Precursor as High-Performance Anode Nanomaterials for Both Li-Ion and Na-Ion Batteries. *Carbon* **2015**, *93*, 143−150.

(7) Mohapatra, L.; Parida, K. A Review on the Recent Progress, Challenges and Perspective of Layered Double Hydroxides as Promising Photocatalysts. *J. Mater. Chem. A* **2016**, *4*, 10744−10766.

(8) Khenifi, A.; Derriche, Z.; Mousty, C.; Prévot, V.; Forano, C. Adsorption of Glyphosate and Glufosinate by Ni2AlNO3 Layered Double Hydroxide. *Appl. Clay Sci.* **2010**, *47*, 362−371.

(9) Feng, L.; Li, A.; Li, Y.; Liu, J.; Wang, L.; Huang, L.; Wang, Y.; Ge, X. A Highly Active CoFe Layered Double Hydroxide for Water Splitting. *Chempluschem* **2017**, *82*, 483−488.

(10) Fagiolari, L.; Scafuri, A.; Costantino, F.; Vivani, R.; Nocchetti, M.; Macchioni, A. A Ternary Zn−Al−Ir Hydrotalcite-Like Compound Exhibiting High Efficiency and Recyclability as a Water Oxidation Catalyst. *Chempluschem* **2016**, *81*, 1060−1063.

(11) Yuan, H.; Wang, Y.; Yang, C.; Liang, Z.; Chen, M.; Zhang, W.; Zheng, H.; Cao, R. Ultra-thin Co−Fe Layered Double Hydroxide Hollow Nanocubes for Efficient Electrocatalytic Water Oxidation. *ChemPhysChem* **2019**, *20*, 2964−2967.

(12) Morales, D. M.; Barwe, S.; Vasile, E.; Andronescu, C.; Schuhmann, W. Enhancing Electrocatalytic Activity through Liquid-Phase Exfoliation of NiFe Layered Double Hydroxide Intercalated with Metal Phthalocyanines in the Presence of Graphene. *ChemPhysChem* **2019**, *20*, 3030−3036.

(13) Felinto Brito, H.; Manoel Loureiro Malta, O.; Claudia França Cunha Felinto, M.; Epaminondas de Sousa Teotonio, E. Luminescence Phenomena Involving Metal Enolates. In *PATAI'S Chemistry of Functional Groups*; John Wiley & Sons, Ltd: Chichester, UK, 2010; pp 131−184.

(14) Binnemans, K. Interpretation of Europium(III) Spectra. *Coord. Chem. Rev.* **2015**, *295*, 1−45.

(15) Lucas, J.; Lucas, P.; Le Mercier, T.; Rollat, A.; Davenport, W. Overview. In *Rare Earths*; Elsevier: Amsterdam, 2015; pp 251−261.

(16) Chang, N. C.; Gruber, J. B. Spectra and Energy Levels of Eu^{3+} in Y_2O_3. *J. Chem. Phys.* **1964**, *41*, 3227−3234.

(17) Bünzli, J. G.; Choppin, G. R. *Lanthanide Probes in Life, Chemical and Earth Sciences Theory and Practice. Spectrochimica Acta Part A: Molecular Spectroscopy*; Elsevier, 1990; p 1797.

(18) Frey, S. T.; Chang, C. A.; Carvalho, J. F.; Varadarajan, A.; Schultze, L. M.; Pounds, K. L.; Horrocks, W. D. Characterization of Lanthanide Complexes with a Series of Amide-Based Macrocycles, Potential MRI Contrast Agents, Using Eu3+ Luminescence Spectroscopy and Molecular Mechanics. *Inorg. Chem.* **1994**, *33*, 2882−2889.

(19) Wu, S. L.; Horrocks, W. D. Kinetics of Complex Formation by Macrocyclic Polyaza Polycarboxylate Ligands: Detection and Characterization of an Intermediate in the Eu^{3+}-Dota System by Laser-Excited Luminescence. *Inorg. Chem.* **1995**, *34*, 3724−3732.

(20) Wu, S. L.; Horrocks, W. D. General Method for the Determination of Stability Constants of Lanthanide Ion Chelates by Ligand−Ligand Competition: Laser-Excited Eu 3+ Luminescence Excitation Spectroscopy. *Anal. Chem.* **1996**, *68*, 394−401.

(21) Wu, S. L.; William DeW. Horrocks, J. Direct Determination of Stability Constants of Lanthanide Ion Chelates by Laser-Excited Europium(III) Luminescence Spectroscopy: Application to Cyclic and Acyclic Aminocarboxylate Complexes. *J. Chem. Soc., Dalton Trans.* **1997**, *9*, 1497−1502.

(22) Lessmann, J. J.; Horrocks, W. D. W. Supramolecular Coordination Chemistry in Aqueous Solution: Lanthanide Ion-Induced Triple Helix Formation. *Inorg. Chem.* **2000**, *39*, 3114−3124.

(23) Voss, D. A.; Farquhar, E. R.; Horrocks, W. D.; Morrow, J. R. Lanthanide(III) Complexes of Amide Derivatives of DOTA Exhibit an Unusual Variation in Stability across the Lanthanide Series. *Inorg. Chim. Acta* **2004**, *357*, 859−863.

(24) Wu, S. L.; Franklin, S. J.; Raymond, K. N.; Horrocks, W. D. Kinetics of the Formation of Macrocyclic Polyaminocarboxylate Ligand Complexes: A Laser-Excited Luminescence Study of the Eu^{3+}−dtpa-Dien System. *Inorg. Chem.* **1996**, *35*, 162−167.

(25) Graeppi, N.; Hugh Powell, D.; Laurenczy, G.; Zékány, L.; Merbach, A. Coordination Equilibria and Water Exchange Kinetics of Lanthanide(III) Propylenediaminetetraacetates and Other Magnetic

Resonance Imaging Related Complexes. *Inorg. Chim. Acta* **1995**, *235*, 311−326.
(26) Albin, M.; Farber, G. K.; Horrocks, W. D. Europium(III) Luminescence Excitation Spectroscopy. A Species-Specific Method for the Quantitation of Lanthanide Ion Binding to Chelating Agents. Complexes of (1,2-Ethanediyldioxy)Diacetate. *Inorg. Chem.* **1984**, *23*, 1648−1651.
(27) Mustafa, D.; Biggemann, D.; Wu, J.; Coffer, J. L.; Tessler, L. R. Structural Characterization of ZnO/ Er2O3 Core/Shell Nanowires. *Superlattices Microstruct.* **2007**, *42*, 403−408.
(28) Moura, R. T.; Carneiro Neto, A. N.; Longo, R. L.; Malta, O. L. On the Calculation and Interpretation of Covalency in the Intensity Parameters of 4f−4f Transitions in Eu 3+ Complexes Based on the Chemical Bond Overlap Polarizability. *J. Lumin.* **2016**, *170*, 420−430.
(29) Gunawan, P.; Xu, R. Lanthanide-Doped Layered Double Hydroxides Intercalated with Sensitizing Anions: Efficient Energy Transfer between Host and Guest Layers. *J. Phys. Chem. C* **2009**, *113*, 17206−17214.
(30) Zhuravleva, N. G.; Eliseev, A. A.; Lukashin, A. V.; Kynast, U.; Tret'yakov, Y. D. Luminescent Materials Based on Tb- and Eu-Containing Layered Double Hydroxides. *Dokl. Chem.* **2004**, *396*, 87−91.
(31) Morais, A. F.; Machado, F. O.; Teixeira, A. C.; Silva, I. G. N.; Breynaert, E.; Mustafa, D. Enhanced Luminescence in ZnAlEu Layered Double Hydroxides with Interlamellar Carboxylate and β-Diketone Ligands. *J. Alloys Compd.* **2019**, *771*, 578−583.
(32) Gao, X.; Hu, M.; Lei, L.; O'Hare, D.; Markland, C.; Sun, Y.; Faulkner, S. Enhanced Luminescence of Europium-Doped Layered Double Hydroxides Intercalated by Sensitiser Anions. *Chem. Commun.* **2011**, *47*, 2104−2106.
(33) Souza, E. R.; Silva, I. G. N.; Teotonio, E. E. S.; Felinto, M. C. F. C.; Brito, H. F. Optical Properties of Red, Green and Blue Emitting Rare Earth Benzenetricarboxylate Compounds. *J. Lumin* **2010**, *130*, 283−291.
(34) Silva, I. G. N.; Brito, H. F.; Souza, E. R.; Mustafa, D.; Felinto, M. C. F. C.; Carlos, L. D.; Malta, O. L. Red (Eu3+), Green (Tb3+) and Ultraviolet (Gd 3+) Emitting Nitrilotriacetate Complexes Prepared by One-Step Synthesis. *Z. Naturforsch., B: J. Chem. Sci.* **2014**, *69*, 231−238.
(35) Gutmann, N. H.; Spiccia, L.; Turney, T. W. Complexation of Cu(II) and Ni(II) by Nitrilotriacetate Intercalated in Zn-Cr Layered Double Hydroxides. *J. Mater. Chem.* **2000**, *10*, 1219−1224.
(36) Kaneyoshi, M.; Jones, W. *Layered Double Hydroxide Intercalate of Metal-Chelate Complex - A Novel Precursor for the Formation of a Mixed Metal Oxide. In Molecular Crystals and Liquid Crystals Science and Technology, Section A: Molecular Crystals and Liquid Crystals*; Gordon and Breach Science Publishers Inc., 2001; Vol. 356, pp 459−468.
(37) Kaneyoshi, M.; Jones, W. Formation of Mg-Al Layered Double Hydroxides Intercalated with Nitrilotriacetate Anions. *J. Mater. Chem.* **1999**, *9*, 805−811.
(38) Gao, R.; Mei, X.; Yan, D.; Liang, R.; Wei, M. Nano-Photosensitizer Based on Layered Double Hydroxide and Isophthalic Acid for Singlet Oxygenation and Photodynamic Therapy. *Nat. Commun.* **2018**, *9*, 1−10.
(39) Marappa, S.; Radha, S.; Kamath, P. V. Nitrate-Intercalated Layered Double Hydroxides - Structure Model, Order, and Disorder. *Eur. J. Inorg. Chem.* **2013**, *12*, 2122−2128.
(40) Gago, S.; Pillinger, M.; Sá Ferreira, R. A.; Carlos, L. D.; Santos, T. M.; Gonçalves, L. S. Immobilization of Lanthanide Ions in a Pillared Layered Double Hydroxide. *Chem. Mater.* **2005**, *17*, 5803−5809.
(41) Duan, X.; Evans, D. G.; He, J.; Kang, Y.; Khan, A. I.; Leroux, F.; Li, B.; Li, F.; O'Hare, D.; Slade, R. C. T.; Taviot-Gueho, C.; Wei, M.; Williams, G. R. Structure and Bonding - Layered Double Hydroxides, 1st ed.; Duan, X.; Evans, D. G., Eds.; Springer, 2005; Vol. *119*.
(42) Pushparaj, S. S. C.; Forano, C.; Prevot, V.; Lipton, A. S.; Rees, G. J.; Hanna, J. V.; Nielsen, U. G. How the Method of Synthesis Governs the Local and Global Structure of Zinc Aluminum Layered Double Hydroxides. *J. Phys. Chem. C* **2015**, *119*, 27695−27707.
(43) Wang, Z.-M.; de Burgt, L. J.; Choppin, G. R. Spectroscopic Study of Lanthanide (III) Complexes with Carboxylic Acids. *Inorg. Chim. Acta* **1999**, *293*, 167−177.
(44) Choppin, G. R.; Bertrand, P. A.; Hasegawa, Y.; RIZKALLAlb, E. N. Thermodynamics of Complexation of Lanthanides by Benzoic and Isophthalic Acids.
(45) *Critical Stability Constants, Amino Acids*, 1st ed.; Martell, A. E.; Smith, R. M., Eds.; Plenum Press: New York, 1974; Vol. *1*.
(46) Gržeta, B.; Lützenkirchen-Hecht, D.; Vrankić, M.; Bosnar, S.; Šarić, A.; Takahashi, M.; Petrov, D.; Bišćan, M. Environment of the Eu3+ Ion within Nanocrystalline Eu-Doped BaAl2O4: Correlation of X-Ray Diffraction, Mössbauer Spectroscopy, X-Ray Absorption Spectroscopy, and Photoluminescence Investigations. *Inorg. Chem.* **2018**, *57*, 1744−1756.
(47) Deacon, G. B.; Phillips, R. J. Relationships between the Carbon-Oxygen Stretching Frequencies of Carboxylato Complexes and the Type of Carboxylate Coordination. *Coord. Chem. Rev.* **1980**, *33*, 227.
(48) Nakamoto, K. *Infrared and Raman Spectra of Inorganic and Coordination Compounds*; John Wiley & Sons, Inc.: Hoboken, NJ, 2008.
(49) Silva, I. G. N.; Cunha, C. S.; Morais, A. F.; Brito, H. F.; Mustafa, D. Eu^{3+}or Sm^{3+}-Doped Terbium-Trimesic Acid MOFs: Highly Efficient Energy Transfer Anhydrous Luminophors. *Opt. Mater.* **2018**, *84*, 123.
(50) Shao, B.; Feng, P.; Wang, X.; Cui, F.; Yang, X. Orientation of (Hetero)Aromatic Anions in the LEuH Interlayer and Enhanced Photoluminescence. *J. Phys. Chem. C* **2019**, *123*, 7467−7474.
(51) Collins, J. M.; Bartolob, B. Di. And Energy Gap Dependence of Energy Transfer Between Rare-Earth Ions in Solids. *J. Lumin.* **1996**, *69*, 335−341.
(52) Yang, G.; Sau, C.; Lai, W.; Cichon, J.; Li, W. The Temperature-Dependence of Multiphonon Relaxation of Rare-Earth Ions in Solid-State Hosts. *J. Phys. Chem. C* **2015**, *344*, 1173−1178.
(53) Mustafa, D.; Silva, I. G. N.; Bajpe, S. R.; Martens, J. A.; Kirschhock, C. E. A.; Breynaert, E.; Brito, H. F. Eu@COK-16, a Host Sensitized, Hybrid Luminescent Metal−Organic Framework. *Dalton Trans.* **2014**, *43*, 13480−13484.
(54) Silva, I. G. N.; Morais, A. F.; Brito, H. F.; Mustafa, D. $Y_2O_2SO_4$:Eu^{3+}Nano-Luminophore Obtained by Low Temperature Thermolysis of Trivalent Rare Earth 5-Sulfoisophthalate Precursors. *Ceram. Int.* **2018**, *44*, 15700−15705.
(55) de Sá, G. F.; Malta, O. L.; de Mello Donegá, C.; Simas, A. M.; Longo, R. L.; Santa-Cruz, P. A.; da Silva, E. F. Spectroscopic Properties and Design of Highly Luminescent Lanthanide Coordination Complexes. *Coord. Chem. Rev.* **2000**, *196*, 165−195.
(56) *The Chemistry of Metal Enolates, Part 1*, 1st ed.; Zabicky, J., Ed.; Wiley: West Sussex, England, 2009.
(57) Silva, I. G. N.; Rodrigues, L. C. V.; Souza, E. R.; Kai, J.; Felinto, M. C. F. C.; Hölsä, J.; Brito, H. F.; Malta, O. L. Low Temperature Synthesis and Optical Properties of the R2O3:Eu3+ Nanophosphors (R3+: Y, Gd and Lu) Using TMA Complexes as Precursors. *Opt. Mater.* **2015**, *40*, 41−48.
(58) Figueroa, S.J.A.; et al. Recent Citations Upgrades to the XAFS2 Beamline Control System and to the Endstation at the LNLS. *J. Phys. Conf. Ser.* **2016**, *712*, No. 012022.
(59) Geng, F.; Xin, H.; Matsushita, Y.; Ma, R.; Tanaka, M.; Izumi, F.; Iyi, N.; Sasaki, T. New Layered Rare-Earth Hydroxides with Anion-Exchange Properties. *Chem. - Eur. J.* **2008**, *14*, 9255−9260.
(60) Ravel, B.; Newville, M. ATHENA, ARTEMIS, HEPHAESTUS: Data Analysis for X-Ray Absorption Spectroscopy Using IFEFFIT. *J. Synchrotron Radiat.* **2005**, *12*, 537−541.
(61) Heiba, Z. K.; Akin, Y.; Sigmund, W.; Hascicek, Y. S. X-Ray Structure and Microstructure Determination of the Mixed Sesqui-oxides (Eu1-XYbx)2O3 Prepared by a Sol-Gel Process. *J. Appl. Crystallogr.* **2003**, *36*, 1411−1416.

https://dx.doi.org/10.1021/acsomega.0c02848
ACS Omega 2020, 5, 23778−23785